Volume 12 | Number 37 | 7 October 2016 | Pages 7701–7874

Soft Matter

www.softmatter.org

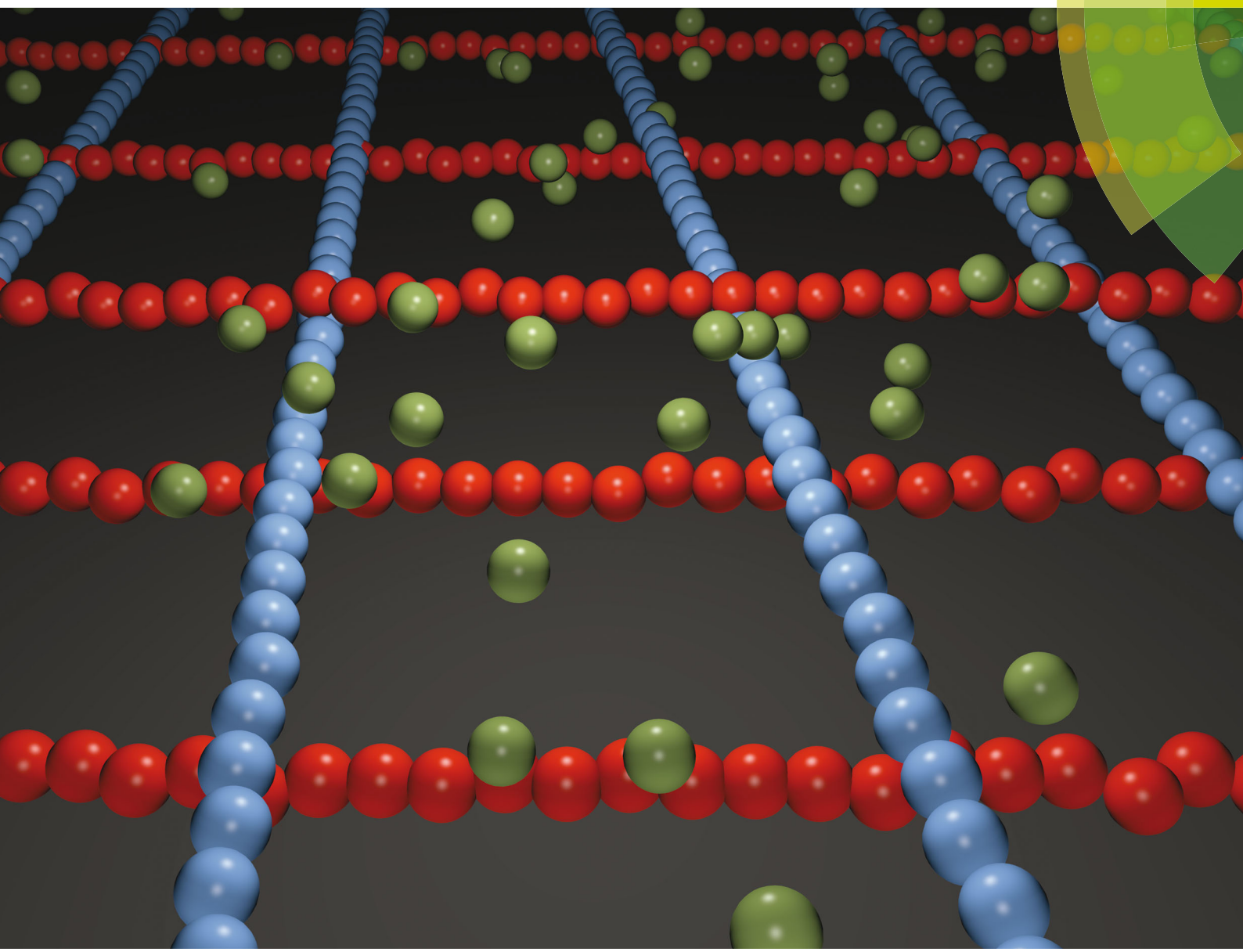

ISSN 1744-683X

ROYAL SOCIETY OF CHEMISTRY

PAPER
Sabine H. L. Klapp, Orlin D. Velev *et al.*
Multidirectional colloidal assembly in concurrent electric and magnetic fields

Soft Matter

PAPER

View Article Online
View Journal | View Issue

Cite this: *Soft Matter*, 2016, 12, 7747

Multidirectional colloidal assembly in concurrent electric and magnetic fields†

Bhuvnesh Bharti,‡§[a] Florian Kogler,‡[b] Carol K. Hall,[a] Sabine H. L. Klapp*[b] and Orlin D. Velev*[a]

Received 26th June 2016,
Accepted 8th August 2016

DOI: 10.1039/c6sm01475e

www.rsc.org/softmatter

Dipolar interactions between nano- and micron sized colloids lead to their assembly into domains with well-defined local order. The particles with a single dipole induced by an external field assemble into linear chains and clusters. However, to achieve the formation of multidirectionally organized nano- or microassemblies with tunable physical characteristics, more sophisticated interaction tools are needed. Here we demonstrate that such complex interactions can be introduced in the form of two independent, non-interacting dipoles (double-dipoles) within a microparticle. We show how this can be achieved by the simultaneous application of alternating current (AC)-electric field and uniform magnetic field to dispersions of superparamagnetic microspheres. Depending on their timing and intensity, concurrent electric and magnetic fields lead to the formation of bidirectional particle chains, colloidal networks, and discrete crystals. We investigate the mechanistic details of the assembly process, and identify and classify the non-equilibrium states formed. The morphologies of different experimental states are in excellent correlation with our theoretical predictions based on Brownian dynamics simulations combined with a structural analysis based on local energy parameters. This novel methodology of introducing and interpreting double-dipolar particle interactions may assist in the assembly of colloidal coatings, dynamically reconfigurable particle networks, and bidirectional active structures.

1. Introduction

Colloidal sized building blocks can be programmed to assemble into ordered macro- and mesoscale structures.[1–5] The physical properties of materials formed on the basis of such structures are governed by the spatial organization of the particles, which can further be altered by changing the interparticle interactions.[6–10] One of the most efficient, robust and widely used methods for directing the colloidal assembly and controlling the interparticle interactions is the application of external electric or magnetic fields.[11–15] Depending upon the physiochemical characteristics of the particles and the applied field(s), the colloids can be assembled into linear chains, 2D or 3D bundles or crystals of desired symmetry.[4,16–20] In the case of isotropic spherical particles, the application of an external field induces a dipole in the particles and lead to their unidirectional chaining.[21–23]

More complex nano- and microscale architectures can be organized with dispersions containing particles of dissimilar polarizability.[24,25] For example, colloidal "flowers" and mixed crystals have been assembled by applying external magnetic fields to bi- or tri-disperse microparticles.[26–28] In these cases, the symmetry of the equilibrium colloidal structure is determined by the strength of the applied field, and the relative magnetic polarizability of the medium and particles. In addition to closed packed structures, mixtures of paramagnetic and diamagnetic colloids have been assembled into a variety of fractal chain assemblies.[28] These aggregates showed growth in parallel and perpendicular directions to the applied magnetic field. Bidirectional chains have been formed due to the presence of anti-parallel dipoles, where the fractal dimension could be tuned by varying the polarizability of the dispersing medium. Such bidirectional chain assemblies are not limited to mixtures of para- and diamagnetic colloids but can also be formed in particle mixtures with dissimilar electrical polarizability (dielectric constant).[29]

Open network structures can also be assembled by applying a high frequency AC-electric field to dispersions of metallodielectric patchy particles with dissimilar local surface polarizabilities.[30] In this case, the bidirectional chaining of patchy particles can

[a] *Department of Chemical and Biomolecular Engineering, North Carolina State University, Raleigh, NC 27695, USA. E-mail: klapp@physik.tu-berlin.de, odvelev@ncsu.edu*
[b] *Institut für Theoretische Physik, PN 7-1, Technische Universität Berlin, Hardenbergstrasse 36, D-10623 Berlin, Germany*

† Electronic supplementary information (ESI) available: Correlation between BD simulations and experiments for various field conditions. Movies illustrating the dynamics of bidirectional particle assembly in experiments (Movie S1), and corresponding BD simulations (Movie S2). See DOI: 10.1039/c6sm01475e

‡ These authors contributed equally to this work.

§ Present address: Cain Department of Chemical Engineering, Louisiana State University, Baton Rouge, LA 70803, USA.

be attributed to the interparticle quadrupolar interactions induced by an external electric field. The assembly of colloids into bidirectional chains and networks is key to the function of electro- and magnetorheological fluids. Having the ability to precisely control the dimension and direction of the colloidal chains/networks provides the basis for developing novel materials with desired anisotropic mechanical and transport properties.[31] We report here how multipolar interactions can be induced and used for colloidal assembly by multiaxial fields instead of using the earlier complex metallodielectric particles with multipolar electrical polarization.[30]

Recently, the use of multiaxial fields have been introduced as a new route to organizing isotropic and anisotropic colloids into crystals, chains and sheets of tunable local symmetry.[32–35] Simultaneous application of a constant and an alternating magnetic field to a dispersion of paramagnetic particles leads to the formation of oscillating chains and colloidal droplets,[36,37] whereas simultaneous graphoepitaxy and electric field application lead to the formation of 2D sheets from orthogonally aligned nanotubes.[31] In both cases the assembled structures consist either of discrete unidirectional chains or closed packed crystals.

In this article we present a new experimental approach where simple superparamagnetic spherical particles are assembled into interconnected well-controlled bidirectional structures by the concurrent application of uniform magnetic and alternating current (AC)-electric fields. The formation of colloidal clusters and bidirectional chains *via* various metastable intermediates is investigated. We interpret the structure of the assemblies formed on the basis of Brownian dynamics (BD) simulations combined with a novel structure analysis method. The latter is based on the examination of energy parameters that probe the local surroundings of the particles.

The application of electric and magnetic fields to magnetic fluids has been shown to introduce interesting optical effects and phase behaviors.[38–40] However, to the best of our knowledge, the combination of the fields has not been used to assemble bidirectional colloidal networks of superparamagnetic microspheres. The biggest advantage of this direct assembly method is the possibility of fine-tuning the assembly morphology by independently varying the electric and magnetic field intensities. We expect that this method will enable multi-parametric control of the physical (*e.g.* rheological, optical) characteristics of the complex fluids, including the selective and unidirectional percolation of 2D networks, controlling the density and stiffness of colloidal gels, and making composite materials with anisotropic shear responses and transport properties. This approach offers a new route for the guided growth of surface coatings with directionally oriented colloidal particles, which otherwise require complex synthetic methods.[41]

2. Results and discussion

The bidirectional assembly of colloids in external electric and magnetic fields was performed on an aqueous dispersion of superparamagnetic microparticles. The microspheres (COMPEL™, Bangs Labs Ltd) contained superparamagnetic nanoparticles embedded in a matrix of polystyrene. The particles had a narrow size distribution in the particle diameter range of $\sigma = 5.7 \pm 0.2$ μm. The particles were strongly negatively charged at pH > 2 because of the surface functionalization with $-COO^-$ groups, and hence they were stable in aqueous dispersion. In a typical experiment, the superparamagnetic microparticle dispersion at pH ~ 6 was transferred to the assembly chamber of the experimental set-up as shown in Fig. 1a. The assembly set-up combined (a) two gold electrodes 2 mm apart for the application of an AC-electric field ($\vec{E}$); and (b) a pair of electromagnets capable of generating a uniform magnetic field ($\vec{H}$) in the range of 10–200 A m^{-1}. The AC electric field was varied in the range of 10–20 V mm^{-1} at a fixed frequency of 10 kHz. These conditions were chosen to minimize AC-electrohydrodynamics, water electrolysis, and other undesired effects on the particle assembly.[22,42,43] The relative angle between the external electric and magnetic fields, 'φ', could be tuned by changing the spatial orientation of the electromagnetic pair with respect to the electrodes (Fig. 1a). In this study we use two different relative field angles $\varphi = 90^\circ$ ($\vec{E} \perp \vec{H}$) and 45°. The change in the spatial distribution of the particles upon the concurrent application was monitored in a direction normal to the assembly plane by a bright-field/fluorescence microscope (Olympus BX-61).

The external field driven assembly of colloids is governed by the field-induced dipolar interactions between the particles.[4,44,45] The effect of the in-plane application of an oscillating electric field can be interpreted as a sheet of current, which means that the oscillation of the electric field induces no magnetic field in the assembly plane.[46] This follows directly from Ampere's law and is important for the decoupling (in plane) of electric and magnetic fields and interactions. Hence, we can reasonably assume that two non-interacting (a) electric and (b) magnetic dipoles are induced in each particle. This configuration of the particles can be termed as a double-dipole state, where each dipole selectively interacts with dipoles of similar type, *i.e.* electric with electric and magnetic with magnetic. These spatially anisotropic particle interactions lead to the formation of bidirectional chains, which exist as long as the external fields are applied. The dipoles and the corresponding attraction between the particles vanish upon switching off the external field(s) and the assembled state reconfigures into its initial disordered state.[47] This assembly-reassembly-disassembly process can be repeated over several cycles without any memory of the initial particle configuration. The general scheme of assembly and reassembly of colloids in the bidirectional field is presented in Fig. 1b.

2.1. Origin of particle interactions in external fields

The morphologies of chain-like colloidal aggregates formed under the action of magnetic and electric fields are markedly different. Optical microscopy images of the assembly of linear chains in an external AC-electric field (zero magnetic field) and the formation of partially staggered chains in a uniform magnetic field (zero electric field) are shown in Fig. 1c and d. This morphological difference originates from the difference in the mechanism of the polarization of the individual particles under

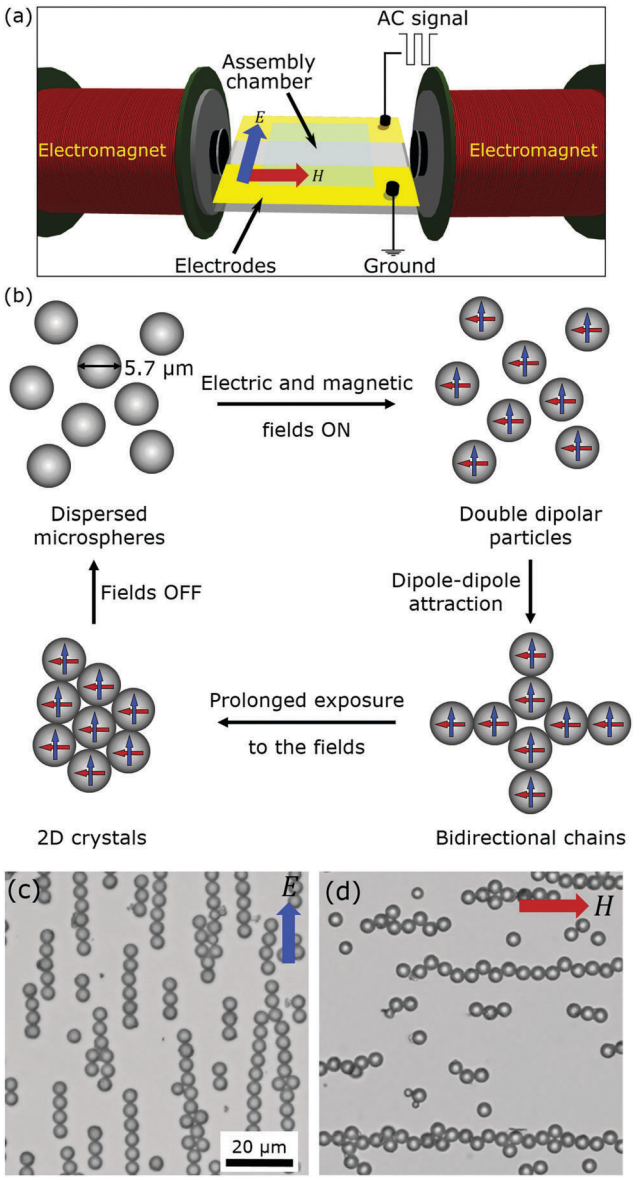

Fig. 1 Schematics of the experimental setup and the concept for bidirectional particle assembly. (a) Setup used for assembling superparamagnetic microspheres by orthogonal AC-electric and constant magnetic field. (b) Schematics of the general approach used for the bidirectional assembly. The electric and magnetic fields were applied simultaneously, inducing two corresponding dipoles in the microspheres. The dipolar interaction drives the particles into cross-chain structures, which slowly re-organize and collapse into 2D crystals after prolonged exposure. Switching off the fields eliminates the interparticle attractions, and the microspheres return to a disordered state. (c) Micrograph of the linear chains formed by superparamagnetic microspheres under an AC-electric field (20 V mm^{-1}, 20 kHz). (d) Partially-staggered chains formed by the application of a uniform magnetic field (125 A m^{-1}). The arrows in (c) and (d) indicate the direction of the applied fields.

external electric and magnetic fields. In the case of the AC-electric field assembly of aqueous colloidal dispersions, the electric dipoles are induced by partial polarization of the counterionic atmosphere around the particles.[11] In this case, the particles can be assumed to have a single dipole which overlaps with the center of mass of the particles. The induced dipole–dipole interaction between particles in an electric field leads to their assembly into linear chains (Fig. 1c).

In a uniform magnetic field, the dipole is induced in the particle by the polarization of the local magnetic domains.[48] In our case of composite microspheres, the magnetic domains are the superparamagnetic nanoparticles embedded in the particles. Hence, the net magnetic dipole moment in a particle is the vector sum of all the individual dipoles induced in the embedded nanoparticles. Depending upon the spatial distribution of the individual magnetic domains in a certain particle, the center of the net magnetic-moment may or may not overlap with its center of mass. This has been shown experimentally for similar superparamagnetic beads.[49] A dislocation of the magnetic dipole from the center of the particle may result in partially staggered chain configurations instead of perfectly linear co-axial chains. We observe that this is also the likely case with our superparamagnetic microparticles, which assemble into linear chains in an external AC-electric field and partially staggered chains in a uniform magnetic field (Fig. 1d). Therefore the networks formed by these off-centered magnetic dipolar particles in concurrent electric and magnetic fields would significantly deviate from the expected checkboard or square-mesh type symmetry.

2.2. Bidirectional particle assembly in electric and magnetic fields

In the absence of any external force, colloidal particles with similar surface charges repel each other and distribute themselves randomly in the dispersion. The simultaneous application of orthogonal electric ($\vec{E}$) and magnetic ($\vec{H}$) fields to the dispersion of superparamagnetic microspheres directs the particles into bidirectional chains. We find that the dynamic process of colloidal assembly results in the formation of bidirectional chains and 2D networks. However, the originally formed structures are metastable and densify after prolonged field exposure time (see Section 2.6 and Movie S1, ESI†). We compare the colloidal assemblies formed after a fixed time at different relative field strengths. The variety of particle structures resulting from the application of different field strengths $\vec{E}$ and $\vec{H}$ after 12 s are illustrated in Fig. 2. The particles form chains in both the $\vec{E}$ (vertical) and $\vec{H}$ (horizontal) directions. The relative population of the particles forming vertical or horizontal chains is governed by the strengths of the two fields (in the cases shown in the figure the magnetic field is slightly dominant).

In our experiments we find that at very low $\vec{E}$ and $\vec{H}$ field strengths, the thermal energy of the particle overcomes the dipolar interaction energy and suppresses the formation of colloidal assemblies. Increasing either field strengths results in the formation of predominantly linear chains aligned in the direction of the respective field; this can be regarded as a string fluid state (Fig. 2i). The assembly of linear chains is solely dominated by the type of dipole–dipole attraction (either electric or magnetic) between the particles. At intermediate strength of both fields, bidirectional dipole–dipole chaining is observed

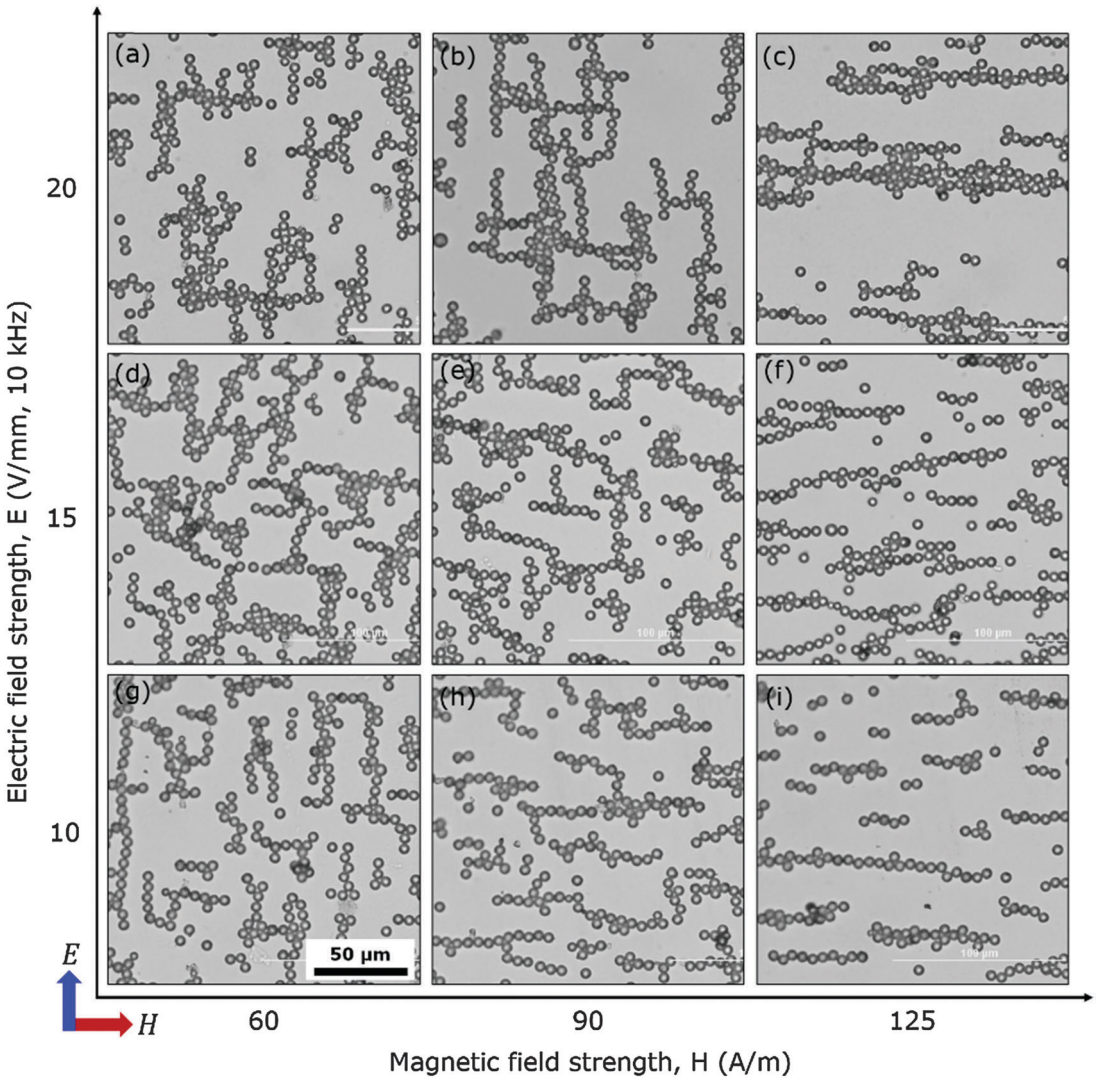

Fig. 2 Bright field optical micrographs of the bidirectional colloidal chain structures formed by superparamagnetic microspheres at different electric (vertical) and magnetic (horizontal) field strengths, $\varphi = 90^\circ$. Here the two fields were applied simultaneously and the images were taken after 12 s of field application. The images indicate that the effective chaining along any direction is determined by the relative intensities of the two fields.

resulting in fine cross-linked particle chains (Fig. 2d and e). Upon increasing the absolute magnitude of both field strengths further, we find the formation of coarse networks with partially crystallized colloidal domains (Fig. 2c). Here the collapsed network formation can be attributed to the (1) lateral interactions between the colloidal chains and (2) rapid assembly and re-assembly of the particle structures (for details see Section 2.6).[37]

2.3. Structural characterization by energy parameters

The application of external electric and magnetic fields could lead to the formation of a variety of structures (see Fig. 3a and b for a representative example). The ordering of particles into 2D networks extends up to several millimeters (Fig. 3a). Here we develop a novel formalism to distinguish between the different network configurations quantitatively. To this end, coordinates of the center of each particle in an experimental microscope image were determined using ImageJ processing software.[50] The resulting colloidal structures are considered as assemblies of constitutive units, each consisting of a central particle with a specific arrangement of nearest neighbors. Particles are considered as neighbors if the spacing between them is less than 1.2σ, where σ is the particle diameter.

The specific constitutive units used for our analysis are shown in Fig. 3c. Depending on the number and spatial orientation of the nearest neighbors, the central particle resides either at the end, or within the horizontal/vertical chains, or it forms a junction of chains. A closer inspection shows that there are eight such constitutive units. We now show that each of these units can be uniquely characterized by a suitably chosen parameter measuring the local electric and magnetic dipolar energies, u_i^{el} and u_i^{mg}, respectively.

In order to fully characterize the assemblies, we assign two dimensionless dipole moments $\boldsymbol{m}^{\alpha}$ (of absolute value 1) to each particle, placed at its center. The first moment points along the

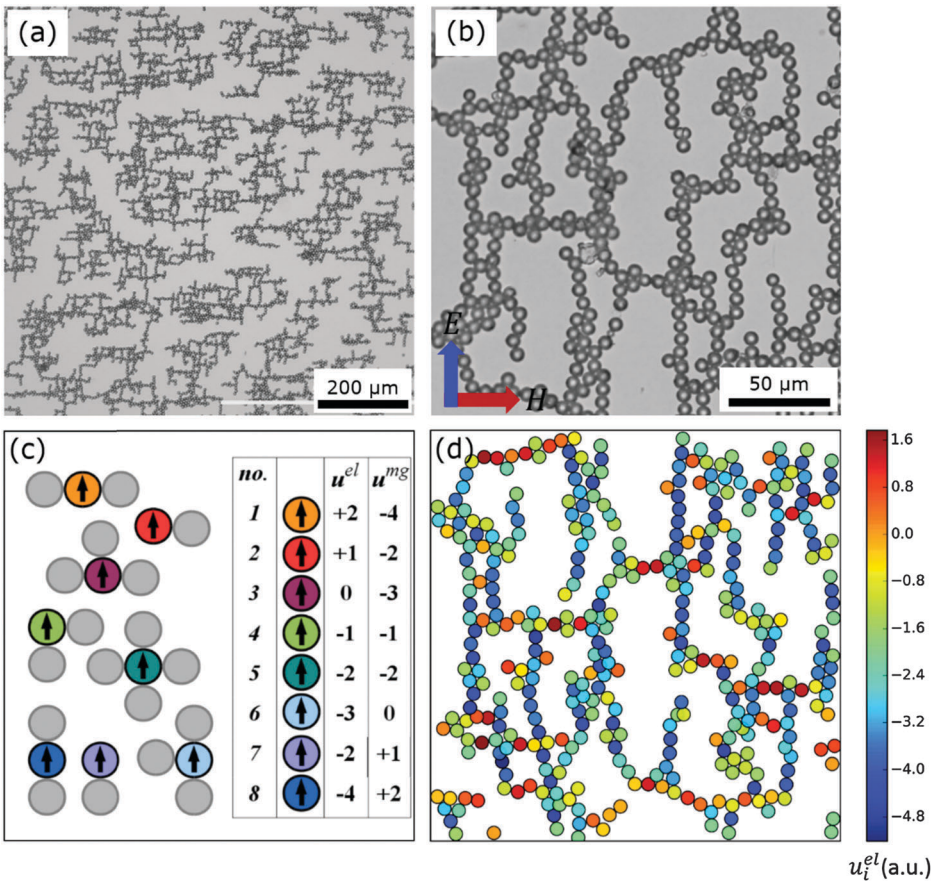

Fig. 3 Colloidal networks formed in concurrent electric and magnetic fields. (a and b) Low and high magnification microscope images of a network formed at E = 20 V mm^{-1} (vertical) and H = 90 A m^{-1} (horizontal). (c) Sketch of the eight constitutive units of particle configurations used in our analysis. Central particles are colored and for simplicity, only the dipole moment $\boldsymbol{m}^{\mathrm{el}}$ along the electric field is indicated. The legend gives the electric and magnetic energy parameter pairs, $(u_i^{\mathrm{el}},u_i^{\mathrm{mg}})$ (see eqn (1)) associated with each unit. (d) Recolored image of the experimental network shown in (b). Each particle is colored according to its electric energy parameter u_i^{el} (see Section 2.3).

electric field (α = el), and the second one points along the magnetic field (α = mg). We note that the unit vectors $\boldsymbol{m}^{\alpha}$ are not the true physical dipole moments governing the assembly process, the latter are introduced in Section 2.4 in the context of our particle-based computer simulations. Here the moments $\boldsymbol{m}^{\alpha}$ serve as tools for our structural analysis. Specifically, we use these quantities to calculate the electric and magnetic pair interaction energy between a particle i and all its N_{b} nearest neighbors *via* the standard formula for dipole–dipole interactions, that is,

$$u_i^{\alpha} = \sum_{j=1}^{N_{\mathrm{b}}} \boldsymbol{m}_i^{\alpha}\boldsymbol{m}_j^{\alpha}e_{ij}^{-3} - 3\left(\boldsymbol{m}_i^{\alpha}\boldsymbol{e}_{ij}\right)\left(\boldsymbol{m}_i^{\alpha}\boldsymbol{e}_{ij}\right)e_{ij}^{-5} \qquad (1)$$

where, $\boldsymbol{e}_{ij}$ is a unit vector directed along the connection vector of the central particle i and its neighbor j. In this way, each particle i is associated with two energy parameters, (a) electric, u_i^{el}; and (b) magnetic, u_i^{mg}. Note that the (dimensionless) interaction energy u_i^{α} between two particles in contact equals −2 in head-to-tail alignment (*i.e.* the connection vector is parallel to the dipole moments) and +1 in head-to-head alignment (*i.e.* the connection vector is perpendicular to the dipole moments).

For example, the central particle in constitutive unit number 1 (see orange particle in Fig. 3c) has two neighbors in the horizontal direction. Since the electric dipole moments $\boldsymbol{m}^{\mathrm{el}}$ are parallel, the central particle is experiencing a repulsive electric dipole–dipole interaction of +1 with each of its neighbors. According to eqn (1), this sums to a total electric energy parameter u_i^{el} = +2. However, the magnetic interaction energy in this configuration is attractive since the magnetic moments $\boldsymbol{m}^{\mathrm{mg}}$ (not shown) are in head-to-tail alignment. Accordingly, each horizontal neighbor in unit number 1 contributes an energy of −2 to the magnetic energy parameter, which therefore sums up to u_i^{mg} = −4. The constitutive unit number 8 (see the bottom of Fig. 3c) represents the opposite situation, where each neighbor contributes −2 due to electric interactions and +1 due to magnetic ones.

As demonstrated by the above example, we can assign a unique pair of energy parameters $(u_i^{\mathrm{el}},u_i^{\mathrm{mg}})$, to each particle in a network (legend of Fig. 3c). Importantly, only the knowledge of both energy parameters allows for a unique identification. For example, knowledge of only one energy parameter is not sufficient to distinguish between a particle at the end of a chain and a particle forming a junction. To illustrate our approach, we determined the parameter pairs $(u_i^{\mathrm{el}},u_i^{\mathrm{mg}})$ for all particles in

the experimental system shown in Fig. 3b. The resulting electric-energy parameters are visualized by the re-colored microscope image in Fig. 3d, where the color code gives the electric energy parameter u_i^{el}. Clearly, particles assembled into vertical chains (along $\vec{E}$) have lower values of u_i^{el} than particles assembled into horizontally aligned chains (along $\vec{H}$). This is because in vertical chains, electric dipoles are aligned head-to-tail whereas magnetic dipoles are aligned head-to-head. The magnetic energy parameter u_i^{mg} for the particles in the network can be calculated and represented in an analogous manner.

Having determined the parameter pair (u_i^{el},u_i^{mg}) for each particle, we can further calculate the distributions of these parameters over the entire network. This provides a quantitative characterization of a given network. An example is shown in Fig. 4a. The peak positions in the distribution plots correspond to particular constitutive units (see Fig. 3c), and the peak heights correspond to their relative population (for a detailed discussion see Section 2.4).

To summarize, our structural analysis allows us to precisely classify the role of each particle in the assembled structure, yielding a detailed quantification in terms of local energies. As we will demonstrate in Section 2.4, this analysis is particularly useful for a detailed comparison between the networks in the experiment, on the one hand, and in the Brownian dynamics simulations, on the other hand. However, to investigate changes in the network structures with external parameters a somewhat coarser level of description turned out to be sufficient. We additionally introduce a simpler classification scheme, where we group together several of the constitutive units introduced before. Specifically, we consider the following three types of particle roles:

(A) Particles in vertical chains (*i.e.*, along the electric field), yielding negative electric interactions and positive magnetic interactions, $u_i^{el} < 0$, and $u_i^{mg} > 0$ (units no. 7 and 8 in Fig. 3c).

(B) Particles in horizontal chains (*i.e.*, along the magnetic field), yielding positive electric interactions and negative magnetic interactions, $u_i^{el} > 0$, and $u_i^{mg} < 0$ (units no. 1 and 2 in Fig. 3c).

(C) Particles forming a junction point or node for interconnected chains, yielding negative or zero values for both energies, $u_i^{el} \leq 0$, and $u_i^{mg} \leq 0$ (units no. 3–6 in Fig. 3c).

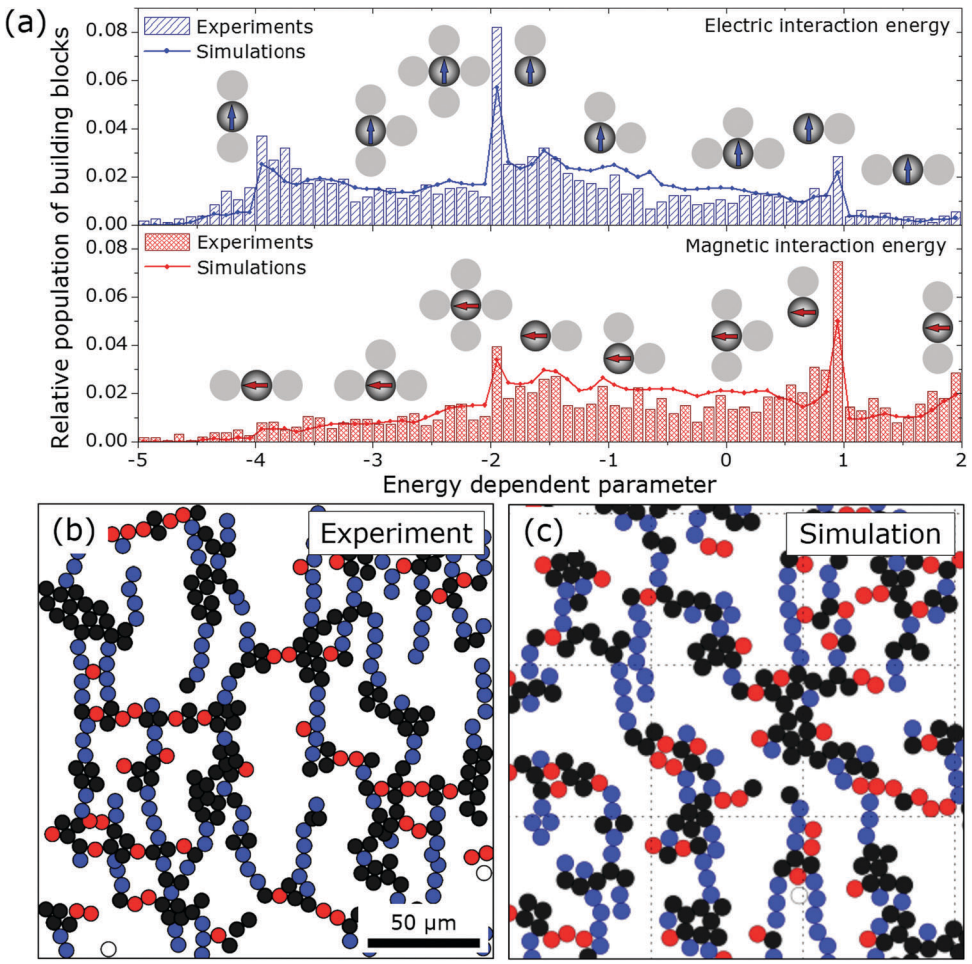

Fig. 4 Comparison of the particle networks formed in experiments and simulations. (a) Distributions of energy parameters u_i^{α} (see eqn (1)) revealing the occurrence of different constitutive units (see Fig. 3c) in the network. The bars correspond to experiments and lines to the Brownian dynamics (BD) simulations. (b) Experimental colloidal network image colored according to the classification introduced in Section 2.3. Type A: vertically chained (blue), type B: horizontally chained (red), and type C: network junctions (black). (c) A snapshot of the BD simulation performed with equal electric and magnetic dipole strength $\langle \mu^{mg} \rangle = \mu^{el} = 0.4$ (a.u.) at reduced number density $\rho^* = 0.35$. The particles in the simulated network are colored as in (b).

This coarser level of classification is especially effective for visual comparison of different particle assemblies. An exemplary structure analyzed by this scheme is shown in Fig. 4b and c, where the particle types A, B and C are colored in red, blue and black, respectively.

2.4. Comparison of experiments and simulations

Bidirectional particle assembly in electric and magnetic fields is a complex phenomenon with several unknown experimental variables. In order to better understand and predict the assembled structures during the course of an experiment, we perform two-dimensional Brownian dynamics (BD) simulations. In a typical simulation run, N_{sp} soft spheres (here $N_{sp} \approx 800$) of diameter σ were placed in a 2D square simulation box of side length L with periodic boundary conditions at constant number density $\rho^* = N_{sp}/(L^2\sigma^2)$. The core–core repulsion between two particles i and j at distance R_{ij} was modeled by a soft-sphere potential, $U_{SS}(R_{ij})$ (for details see Appendix) with the interaction energy parameter ε serving as a unit of energy. The electric field induced interactions are modeled by placing a point dipole moment $\boldsymbol{\mu}_i^{el}$, with fixed orientation along the electric field, in the center of each particle i (Fig. 8). Dipole moments are given in units of $\sqrt{\sigma^3\varepsilon}$.

To account for magnetic interactions, each particle bears additionally a magnetic dipole $\boldsymbol{\mu}_i^{mg}$ pointing along the magnetic field (Fig. 8). In our experiments, the microparticle is made of several magnetic microdomains (made of the magnetic particles dispersed inside the polymer core). In the simulations, for simplicity we assume that a single magnetic dipole represents the net vector sum of all magnetic microdomains and captures the essence of magnetic interactions between the particles. As indicated in Section 2.1, the position of the magnetic dipole in this type of experimental system may not overlap with the particles' center of mass. In principle, the magnetic dipole may be present anywhere within the particle, but for simplicity we place it randomly on a circle around the particle center and denote its displacement from the center by a vector $\boldsymbol{\delta}_i$ with absolute value $\delta = 0.2\sigma$ and random direction. The absolute value of each magnetic moment is chosen from a Gaussian distribution with mean value $\langle\mu^{mg}\rangle$ and variance $\langle\mu^{mg}\rangle/2$, which accounts for imperfections in the process of producing the particles.

The dipolar interaction between particle i and j due to the magnetic or electric dipoles is calculated according to the long-ranged point dipole–dipole potential

$$U_{dip}^{\alpha}(\boldsymbol{r}_{ij}) = \boldsymbol{\mu}_i^{\alpha}\cdot\boldsymbol{\mu}_j^{\alpha}/r_{ij}^{3} - 3(\boldsymbol{\mu}_i^{\alpha}\cdot\boldsymbol{r}_{ij})(\boldsymbol{\mu}_j^{\alpha}\cdot\boldsymbol{r}_{ij})/r_{ij}^{5} \quad (2)$$

where the superscript α = el or mg indicates either electric or magnetic dipoles. In the latter case, the distance vector is a function of the random shift, *i.e.* $\boldsymbol{r}_{ij} = \boldsymbol{r}_{ij}(\boldsymbol{\delta}_i,\boldsymbol{\delta}_j)$ (see Appendix). The net interaction energy between two particles is given by

$$U_{ij}(\boldsymbol{r}_{ij}) = U_{SS}(R_{ij}) + U_{dip}^{el}(\boldsymbol{r}_{ij}) + U_{dip}^{mag}(\boldsymbol{r}_{ij}) \quad (3)$$

where R_{ij} is the distance between the particle's centers-of-mass. The potential is visualized in Fig. 8 (see Appendix). We use standard two-dimensional Ewald summation to incorporate long-ranged dipolar interactions.[51] For further details on simulations and their comparison with experiments see Appendix and the ESI† (Fig. S1).

2.5. Construction of operational state diagram

The simultaneous application of electric and magnetic fields is an unusual method for organizing colloids into bidirectional chains, networks, and clusters. We find that the morphologies of assembled structures in biaxial fields are highly dependent on the number density of particles and on the initial configurations. We note that in experiments the number density of the assembling particles is subject to stochastic variations between different experiments. In the present study, computer simulations allow us to overcome this difficulty and investigate the state of assembly at a given time with a precise control over the particle density. Here we used Brownian dynamics (BD) simulations to construct a non-equilibrium state diagram of different assembled morphologies, evaluated in a particular time interval $t = [8,12]\tau_B$, where τ_B is the Brownian time scale (see Appendix). Note that the simulated network structures are transient and collapse over time, similar to what happens in experiment (for details see Section 2.6, and Movie S2, ESI†). A quantitative connection could not be established.

As described at the end of Section 2.3, the particles can be sorted into three types A, B, and C according to their roles in the network. In order to quantify their relative population at different external field parameters, we identify the number of particles forming horizontal chains N_B – (red colored in Fig. 4b and c), vertical chains N_A – (blue colored in Fig. 4b and c), and junction points or nodes N_C – (black colored in Fig. 4b and c), such that $N = N_A + N_B + N_C$, where N is the total number of assembled particles with at least one neighbor. Based on these numbers, we sort the multi-particle assemblies formed under various field configurations into four different categories as shown in Table 1.

The predominant fraction of these four types of particle states is governed by the relative electric and magnetic field strengths (for details see Section 2.5). The state diagram shown in Fig. 5a is constructed from a set of BD simulations with a constant particle number density $\rho^* = 0.35$ with the constraint that at least 70% of the particles attain an assembled state (*i.e.* minimum one neighbor). At very low field strengths (or moment), no significant assembly was observed (Fig. 5a). In the extreme case where one of the fields is much stronger than the other, the assembled configuration is a string fluid phase (state I or II, Fig. 5a and b) oriented in the direction of the dominant field. However, as discussed previously the locally assembled state of the particle in external electric and magnetic fields differs slightly, being in linear and partially staggered chains respectively (states I and II, see Section 2.3). A more versatile behavior is observed when the two moments generated in the particle by electric and magnetic fields are similar in magnitude. When the absolute values of the two moments (μ^{el} and $\langle\mu^{mg}\rangle$) are comparable, but are less than $0.5\sqrt{\sigma^3\varepsilon}$, a fine bidirectional low-density gel structure is obtained (state III). However, if the two moments are increased in their absolute magnitudes, a coarser structure with more compact particle packing is observed (state IV). In this state, small domains

Table 1 Characterizing the type of assembled network structure on the basis of the number of particles involved in vertical (N_A) and horizontal (N_B) chains, and in junction points (N_C). The total number of particles with at least one neighbor is N

State	Type of structure	Condition
I	Vertical string fluid	$N_A > (N_B + N_C)$
II	Horizontal string fluid	$N_B > (N_A + N_C)$
III	Fine networks	$(N_B + N_A) > N_C$ and $N_A < (N_B + N_C)$ and $N_B < (N_A + N_C)$
IV	Coarse networks	$(N_B + N_A) < N_C$

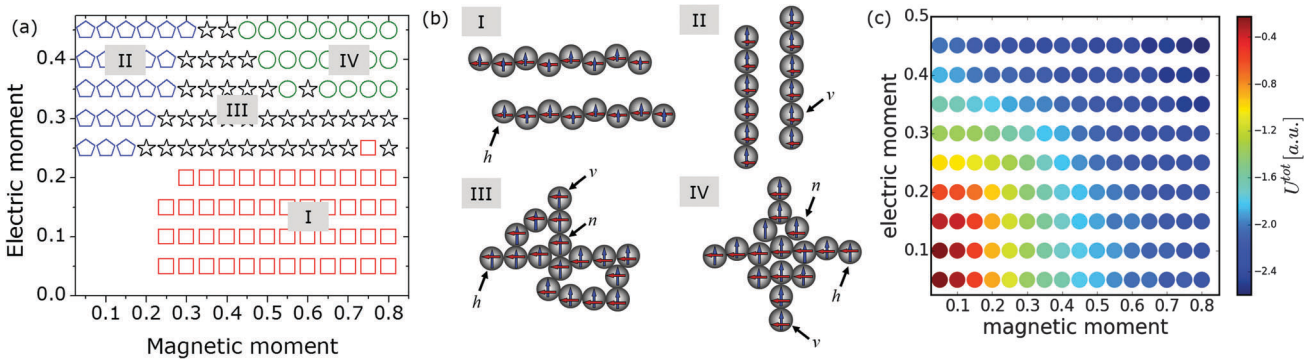

Fig. 5 State diagram of the colloidal particles in bidirectional electric and magnetic fields. (a) The non-equilibrium state diagram of the particles at number density $\rho^* = 0.35$ as established by Brownian dynamics simulations. The states where >70% of particles are assembled (*i.e.* have at least one neighbor) are shown in the diagram. (b) Schematic representation of the four distinct states (or structures) identified in the simulations. The detailed criteria for distinguishing different states are given in Table 1. (c) Total energies associated with the data points in part (a), obtained according to eqn (1). The magnitude is shown by the color bar on the right.

of colloidal clusters are interconnected *via* particle chains and the state can be regarded as a high-density gel.

The formation of coarse gel structures in state IV as compared to the fine bidirectional chains (state III) can be attributed to the kinetic entrapment of particles into closed packed configurations at elevated field strengths. At this point, it should be mentioned that the distinction between the structures is given by a change in the population of particles in different roles. Thus, the state 'boundaries' shown in Fig. 5a are only estimates since the transition between states is gradual. The detection of this smooth crossover in experiment is not possible as it is very sensitive to density variations. These gradual transitions between the different states are also reflected by the plot of the total energies (evaluated by summing over all individual energies eqn (1), *i.e.* $U^{\mathrm{tot}} = \frac{1}{N}\sum_{i=1}^{N}\sum_{\alpha=\mathrm{el,mg}} u_i^{\alpha}$). As expected, the largest energies are found in the most correlated state IV (Fig. 5c). However, the crossover towards the states I–III is rather smooth. Only for small values of the two moments the total energies are significantly different (*i.e.* much closer to zero), reflecting an absence of dipole-induced clusters (Fig. 5c).

2.6. Collapse of colloidal networks into 2D crystals

The formation of particle bidirectional networks in electric and magnetic fields is a non-equilibrium process and the initially formed metastable structures dynamically reconfigure with prolonged exposure to the fields. Upon the concurrent application of orthogonal $\vec{E}$ and $\vec{H}$ fields, randomly dispersed microspheres first assemble into fine colloidal networks and then the networks collapse into discrete clusters (Fig. 6a–f). Here we characterize the kinetics of this particle reorganization in terms of the change in the number of nearest neighbors of a particle with time (Fig. 6g). During the course of the reassembly, the population of particles with a higher number of immediate neighbors increases at the expense of particles with a lower number of nearest neighbors. As mentioned in the previous sections, the formation of bidirectional chains can be attributed to the head-to-tail particle interactions induced by the orthogonal electric and magnetic dipoles. However, the collapse of the chains into discontinuous colloidal crystals (2D droplets) is the result of the lateral rearrangement leading to the maximization of these dipolar interactions around each particle.[52] Previously it has been shown that such lateral interactions between dipolar colloids lead to the formation of multiparticle thick coarse chains and 2D clusters.[22,53]

However in our case of double dipoles, this sprawling of the clusters is lost and the particles collapse into "droplets" of closed packed microspheres. The increase in the population of particles with six neighbors (Fig. 6g inset) confirms this behavior. We also note that the simulated structures collapse over time in qualitative agreement with the experiment. This is illustrated in Fig. 6h, where we plot the time dependence of the number of particles with 4–6 (and zero) neighbors. Qualitatively, the behavior is similar to what is seen in experiment. Moreover, the simulations clearly show that the collapse is accompanied by a marked decrease of the total energy U^{tot} (Fig. 6h inset).

2.7. Versatility of the biaxial field assembly approach: non-orthogonality and particle mixtures

The formation of multidirectional assemblies by superparamagnetic microspheres in combined electric and magnetic

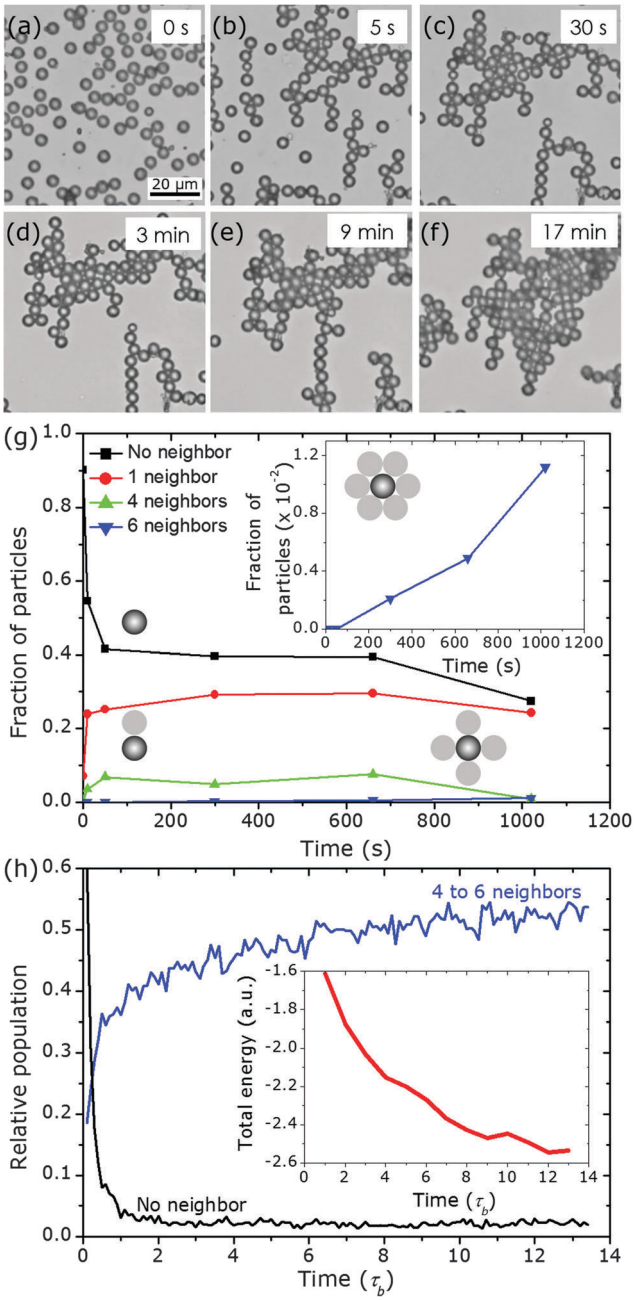

Fig. 6 Time dependent reconfiguration of the particle network in bidirectional fields. (a–f) Experimental images showing the formation and internal collapse of particle networks into 2D hexagonal crystals. The collapse is observed only after prolonged application of electric and magnetic fields. (g) The change in the relative population of particles with different numbers of immediate neighbors during the collapse process. The fraction of particles in the non-assembled state (singles) decreases and the population of particles with six neighbors (inset) increases indicating the formation of 2D hexagonal structures over time. (h) Time dependence of the number of particles with 4–6 and with no neighbors at number density $\rho^* = 0.35$ and equal magnetic and electric dipole moments ($\langle\mu^{mg}\rangle = \mu^{el} = 0.45$) in Brownian dynamics simulations. The inset shows the time dependence of the total energy U^{tot} (see Section 2.5).

fields is not limited to orthogonal chaining. More complex structures can be assembled by changing the parameters of the applied field. Up to this point, we have investigated the formation of bidirectional chains from monoparticle dispersions in mutually orthogonal ($\varphi = 90^\circ$) applied electric and magnetic fields. Altering the relative angle between the two fields would change the mutual direction of the local particle interactions, which results in a more complex colloidal assembly process. One such example of the assembly of a monoparticle dispersion in non-orthogonal fields is shown in Fig. 7a. Unlike bidirectional chain assembly in orthogonal fields when $\varphi = 90^\circ$, the particles show the formation of elongated 2D-hcp crystals for a field angle of $\varphi = 45^\circ$. The dipole–dipole interaction between two particles remains attractive until the angle between the applied field vector and the line joining the induced dipole centers is $<54^\circ$.[54] When the induced dipoles in a particle are orthogonal and off-centered, distinct regions of attraction and repulsion are created around a particle (Fig. 8 in the Appendix).[55] However, changing the relative orientation of the two dipoles may result in a complex surface interaction pattern around the particles. The formation of the closed packed clusters in experiments demonstrates that the spatial interaction is more isotropic in the case of electric and magnetic fields mutually inclined at 45° in comparison to 90°. Further experimental and simulation studies would be necessary to understand the origin of this behavior, which are beyond the scope of the present work.

Further complexity in the assembled structures can be achieved by using a mixture of particles with dissimilar polarizabilities. For example, we use a mixture of superparamagnetic and non-magnetic microspheres of ~3 μm diameter each (Fig. 7b). Upon simultaneous application of $\vec{E}$ and $\vec{H}$, the superparamagnetic colloids acquired double-dipoles, while the non-magnetic particles develop only a single electric dipole. The assemblies formed by the mixture of these particles under orthogonal electric and magnetic fields ($\varphi = 90^\circ$) are shown in Fig. 7c. The superparamagnetic particles (green) are aligned in the direction of $\vec{H}$ (horizontal) and the non-magnetic microspheres (red) form chains in the direction of $\vec{E}$ (vertical). Similar to the assemblies formed by the only superparamagnetic particles in bidirectional fields, we observe interconnected chains of magnetic and non-magnetic particles. The chains of superparamagnetic and non-magnetic particles interconnect solely due to electric dipole interactions. One major difference between the structures formed by the biparticle dispersion and the monoparticles (see Sections 2.2–2.6) is the ability to independently control the degree of particle chaining in the latter case. Furthermore, the assemblies formed by the biparticle dispersion at $\varphi = 45^\circ$ differ significantly from the coarse chains and colloidal "droplets" formed in monoparticle dispersions (Fig. 7a and d). The biparticle dispersion at $\varphi = 45^\circ$ assembles into 'fishnet' type interconnected chains and linear clusters. This network assembly of inclined chains is possible only in the case of biparticle dispersions with dissimilar particle polarizability under concurrent electric and magnetic fields, which otherwise would either assemble into 2D colloidal crystals or orthogonal chains. In this case, the spatial interactions between non-magnetic particles remain highly anisotropic because of the presence of a single electric dipole. This anisotropy restricts the formation of closed packed structures, which otherwise would lead to the formation of 2D hcp crystals as shown in Fig. 7a.

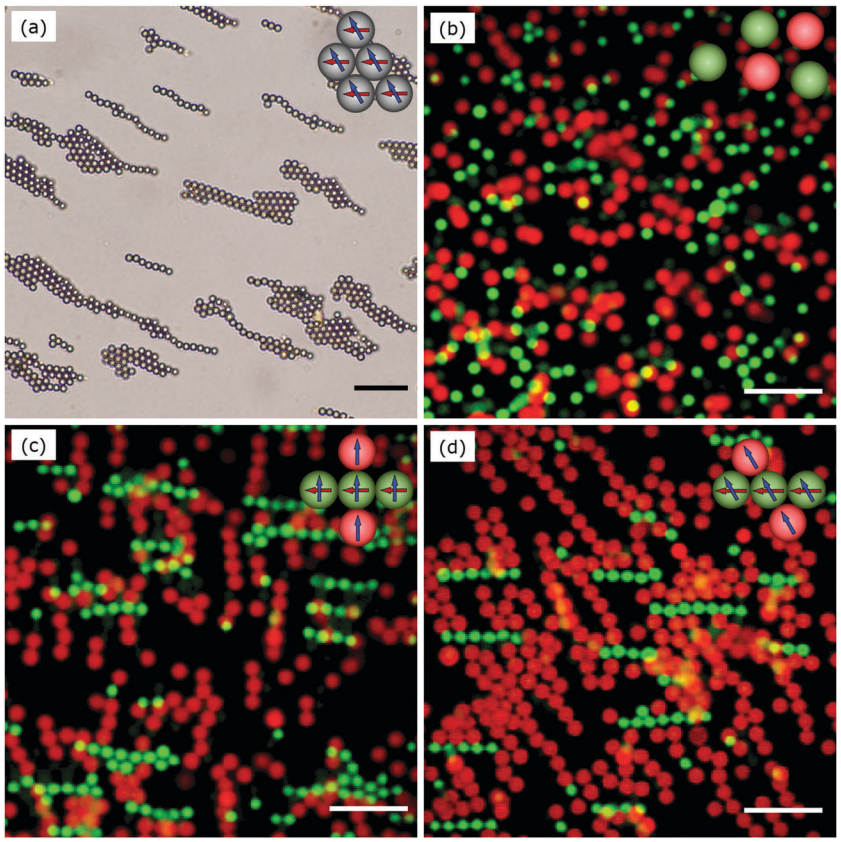

Fig. 7 Examples of complex colloidal assemblies formed in non-orthogonal pairs of electric and magnetic fields. (a) Compact 2D crystals formed by a monoparticle superparamagnetic microsphere dispersion in electric and magnetic fields inclined at an angle φ = 45°. Bidirectional chains and interconnected networks are absent in this case. (b) A random distribution of superparamagnetic (green) and non-magnetic (red) microparticles in an aqueous dispersion in the absence of external fields. (c) Bidirectional colloidal particle chains formed by mixed dispersion (b) under the application orthogonal magnetic (horizontal) and electric (vertical) fields. (d) The mixture of particles assembled into 'fish-net' type bidirectional chain structures upon simultaneous application of $\vec{E}$ and $\vec{H}$ inclined at an angle of 45°. Unlike the monoparticle dispersion, the mixed particles form interconnected chains in non-orthogonal (here φ = 45°) fields. Scale bars = 20 μm.

Multi-field induced interactions combined with multiple types of particles offer new opportunities to guide the growth of 2D networks and chain-like assemblies. The finite kinetics of assembly allows the possibility of arresting and preserving the network structure at any stage of the process by rapid polymerization or freezing of the surrounding media.[56,57] Techniques such as transfer printing can be further used to transform these bidirectional chains into new materials and devices.[58] Furthermore, these colloidal assemblies when immobilized within a thermo-responsive hydrogel can direct soft material bending upon thermally induced gel shrinking.[56,59] Hence, various forms of reconfigurable metamaterials can be assembled by engineering the constituent particle interactions and spatial distributions *via* a combination of electric and magnetic fields.

3. Conclusions

We used a new experimental method for assembling colloidal particles into bidirectional chains and 2D clusters, and developed a novel theoretical approach to interpret and understand the colloidal structures formed. The results demonstrate how superparamagnetic microbeads in aqueous dispersion can be assembled into interconnected chain networks using orthogonal electric and magnetic fields. This process is highly dynamic; the assembled states are of transient nature and eventually reconfigure into closed packed crystals. In order to better understand the mechanism of network formation, we performed Brownian dynamics simulations and developed a sophisticated strategy to characterize the networks' topological features based on energy criteria. This method of analysis is easily transferable to other types of colloidal networks. Based on our simulations, we presented a state diagram of the assembled structures which identifies four types of structures that form during the assembly process, namely: (1 and 2) string fluid with vertical and horizontal chains with no interconnectivity; (3) fine-gel networks with single particle chains in two directions; and (4) coarse-gel with discrete particle clusters attached with colloidal chains. These four types of structures could result in distinctly different types of materials, if the networked particles are bound or embedded in an external host matrix. In addition to these networks, we experimentally showed that more complex assemblies can be formed by changing the relative angle between the applied fields and by incorporating mixtures of particles with different polarizability behaviors in the fields. We believe that this approach of

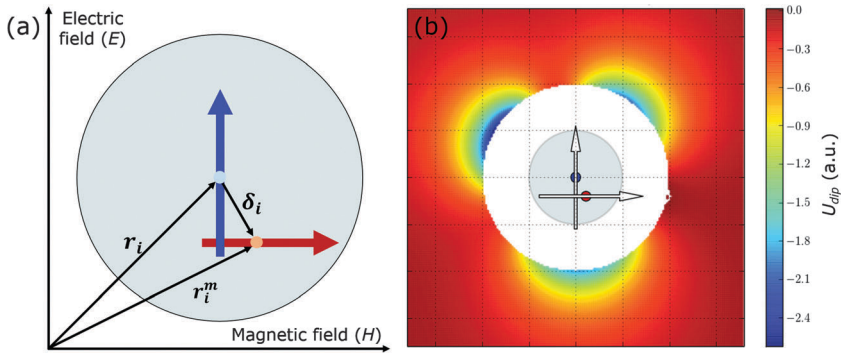

Fig. 8 The basics of the double dipolar model used for the BD simulations. (a) The schematic representation of a single particle with two independent non-interacting point dipoles. (b) The energy map of the double dipolar particles.

particle assembly is generic and can be universally applied to a variety of colloidal dispersions. Hence, this methodology of assembling colloids could enable the controlled formation of a broad range of colloidal materials comprising bidirectional chains and colloidal clusters.

Appendix

Simulation details

The repulsive interaction between two particles (i and j) was modeled by a shifted Lennard-Jones potential.

$$U_{SS}(R_{ij}) = 4\varepsilon\left(\left(\frac{\sigma}{R_{ij}}\right)^{12} - \left(\frac{\sigma}{R_{ij}}\right)^{6}\right) + \varepsilon \text{ for } R_{ij} < 2^{1/6}\sigma \quad \text{(A1)}$$

Here, ε is the interaction strength parameter, σ is the particle diameter and R_{ij} is the center-to-center distance between particles i and j. Truncating the potential at $R_{ij}^{SS} = 2^{1/6}\sigma$ results in solely repulsive interactions.

The distance between dipole moments $\boldsymbol{\mu}_i^{\alpha}$ and $\boldsymbol{\mu}_j^{\alpha}$ of the same species α = (el, mg) depends on the species (Fig. 8). It is given by $\boldsymbol{r}_{ij} = \boldsymbol{r}_i - \boldsymbol{r}_j + \boldsymbol{\delta}_j - \boldsymbol{\delta}_i$ for the magnetic case (α = mg). For electric interactions (α = el) it is given by $\boldsymbol{r}_{ij} = \boldsymbol{r}_i - \boldsymbol{r}_j$ (corresponds to $\boldsymbol{\delta}_{i,j} = 0$) and equals the center-of-mass distance.

We perform overdamped Brownian dynamics simulations with the equations of motion

$$\gamma\dot{\boldsymbol{r}}_i = \sum_{j=1}^{N} \nabla_{\boldsymbol{r}_{ij}} U(R_{ij}, \boldsymbol{r}_{ij}) + \boldsymbol{\zeta}_i \quad \text{(A2)}$$

where γ is the friction constant and $\boldsymbol{\zeta}_i$ is a Gaussian noise vector acting on particle i and fulfilling $\langle\boldsymbol{\zeta}_i\rangle = 0$ and $\langle\boldsymbol{\zeta}_i(t)\boldsymbol{\zeta}_j(t')\rangle = 2\gamma T^*\delta_{ij}\delta(t - t')$ with $T^* = k_BT/\varepsilon$ being the temperature times Boltzmann's constant in units of ε. In all simulations holds $T^* = 0.1$. Eqn (A1) and (A2) are solved *via* the Euler scheme with an integration step width $\Delta t = 10^{-5}\tau_B$, where τ_B is a Brownian time scale defined by $\tau_B = \sigma^2\gamma/\varepsilon T^*$.

Acknowledgements

We are thankful to Ncamisile Maseko and Shan Zhu for assistance with the preparatory experimental work. BB, CKH, and ODV gratefully acknowledge the financial support from the Research Triangle NSF MRSEC on Programmable Soft Matter (DMR-1121107). BB and ODV also acknowledge support from the US NSF-CBET division (CBET-1604116). FK and SHKL thank the German Research Foundation (DFG) under the framework of IRTG-1524 for financial support.

References

1 M. Grzelczak, J. Vermant, E. M. Furst and L. M. Liz-Marzán, *ACS Nano*, 2010, **4**, 3591–3605.
2 G. M. Whitesides and B. Grzybowski, *Science*, 2002, **295**, 2418–2421.
3 J. Lim, C. Lanni, E. R. Evarts, F. Lanni, R. D. Tilton and S. A. Majetich, *ACS Nano*, 2011, **5**, 217–226.
4 O. D. Velev and S. Gupta, *Adv. Mater.*, 2009, **21**, 1897–1905.
5 T. C. Shyu, P. F. Damasceno, P. M. Dodd, A. Lamoureux, L. Xu, M. Shlian, M. Shtein, S. C. Glotzer and N. A. Kotov, *Nat. Mater.*, 2015, **14**, 785–789.
6 L. Cademartiri and K. J. M. Bishop, *Nat. Mater.*, 2015, **14**, 2–9.
7 D. Zerrouki, J. Baudry, D. Pine, P. Chaikin and J. Bibette, *Nature*, 2008, **455**, 380–382.
8 D. J. Kraft, R. Ni, F. Smallenburg, M. Hermes, K. Yoon, D. A. Weitz, A. van Blaaderen, J. Groenewold, M. Dijkstra and W. K. Kegel, *Proc. Natl. Acad. Sci. U. S. A.*, 2012, **109**, 10787–10792.
9 F. L. Yap, P. Thoniyot, S. Krishnan and S. Krishnamoorthy, *ACS Nano*, 2012, **6**, 2056–2070.
10 F. Martinez-Pedrero, A. Cebers and P. Tierno, *Soft Matter*, 2016, **12**, 3688–3695.
11 B. Bharti and O. D. Velev, *Langmuir*, 2015, **31**, 7897–7908.
12 K. D. Hermanson, S. O. Lumsdon, J. P. Williams, E. W. Kaler and O. D. Velev, *Science*, 2001, **294**, 1082–1086.
13 A. Cebers and K. Erglis, *Adv. Funct. Mater.*, 2016, **26**, 3783–3795.
14 R. M. Erb, J. J. Martin, R. Soheilian, C. Pan and J. R. Barber, *Adv. Funct. Mater.*, 2016, **26**, 3859–3880.
15 D. Li, J. Rogers and S. L. Biswal, *Langmuir*, 2009, **25**, 8944–8950.
16 J. J. Crassous, A. M. Mihut, E. Wernersson, P. Pfleiderer, J. Vermant, P. Linse and P. Schurtenberger, *Nat. Commun.*, 2014, **5**, 5516.

17 B. Bharti, A.-L. Fameau, M. Rubinstein and O. D. Velev, *Nat. Mater.*, 2015, **14**, 1104–1109.
18 M. Wang, L. He, W. Xu, X. Wang and Y. Yin, *Angew. Chem., Int. Ed.*, 2015, **54**, 7077–7081.
19 T. Mohorič, J. Dobnika and J. Horbach, *Soft Matter*, 2016, **12**, 3142–3148.
20 J. A. Ferrar and M. J. Solomon, *Soft Matter*, 2015, **11**, 3599–3611.
21 B. Bharti, G. H. Findenegg and O. D. Velev, *Langmuir*, 2014, **30**, 6577–6587.
22 S. O. Lumsdon, E. W. Kaler and O. D. Velev, *Langmuir*, 2004, **20**, 2108–2116.
23 A. P. Hynninen and M. Dijkstra, *Phys. Rev. Lett.*, 2005, **94**, 8–11.
24 I. Kretzschmar and J. H. (Kevin) Song, *Curr. Opin. Colloid Interface Sci.*, 2011, **16**, 84–95.
25 S. K. Smoukov, S. Gangwal, M. Marquez and O. D. Velev, *Soft Matter*, 2009, **5**, 1285–1292.
26 R. M. Erb, H. S. Son, B. Samanta, V. M. Rotello and B. B. Yellen, *Nature*, 2009, **457**, 999–1002.
27 Y. Yang, L. Gao, G. P. Lopez and B. B. Yellen, *ACS Nano*, 2013, **7**, 2705–2716.
28 J. Byrom and S. L. Biswal, *Soft Matter*, 2013, **9**, 9167–9173.
29 B. Bharti and O. D. Velev, *Z. Phys. Chem.*, 2015, **229**, 1075–1088.
30 S. Gangwal, A. Pawar, I. Kretzschmar and O. D. Velev, *Soft Matter*, 2010, **6**, 1413–1418.
31 A. Ismach and E. Joselevich, *Nano Lett.*, 2006, **6**, 1706–1710.
32 M. E. Leunissen, H. R. Vutukuri and A. van Blaaderen, *Adv. Mater.*, 2009, **21**, 3116–3120.
33 S. H. L. Klapp, *Curr. Opin. Colloid Interface Sci.*, 2016, **21**, 76–85.
34 F. Smallenburg and M. Dijkstra, *J. Chem. Phys.*, 2010, **132**, 204508.
35 S. Jäger and S. H. L. Klapp, *Soft Matter*, 2011, **7**, 6606–6616.
36 J. W. Swan, J. L. Bauer, Y. Liu and E. M. Furst, *Soft Matter*, 2014, **10**, 1102–1109.
37 J. W. Swan, P. A. Vasquez, P. A. Whitson, E. M. Fincke, K. Wakata, S. H. Magnus, F. D. Winne, M. R. Barratt, J. H. Agui, R. D. Green, N. R. Hall, D. Y. Bohman, C. T. Bunnell, A. P. Gast and E. M. Furst, *Proc. Natl. Acad. Sci. U. S. A.*, 2012, **109**, 16023–16028.
38 V. V. Chenkov, V. M. Kozhenvnikov, V. V. Padalka and N. Skibin, Yu., *Magnetohydrodynamics*, 1985, **2**, 79–83.
39 Y. I. Dikansky and O. A. Nechaeva, *Magnetohydrodynamics*, 2001, **37**, 394–397.
40 Y. I. Dikansky and O. A. Nechaeva, *Magnetohydrodynamics*, 2002, **38**, 287–291.
41 D. Tsivion, M. Schvartzman, R. Popovitz-Biro and E. Joselevich, *ACS Nano*, 2012, **6**, 6433–6445.
42 P. P. Lele, M. Mittal and E. M. Furst, *Langmuir*, 2008, **24**, 12842–12848.
43 S. Gupta, R. G. Alargova, P. K. Kilpatrick and O. D. Velev, *Langmuir*, 2010, **26**, 3441–3452.
44 F. Smallenburg, H. R. Vutukuri, A. Imhof, A. van Blaaderen and M. Dijkstra, *J. Phys.: Condens. Matter*, 2012, **24**, 464113.
45 A. A. Shah, B. Schultz, W. Zhang, S. C. Glotzer and M. J. Solomon, *Nat. Mater.*, 2015, **14**, 117–124.
46 D. J. Griffiths, *Introduction to Electrodynamics*, Addison-Wesley, 4th edn, 2012.
47 B. Bharti, G. H. Findenegg and O. D. Velev, *Sci. Rep.*, 2012, **2**, 1004.
48 B. Ren, A. Ruditskiy, J. H. K. Song and I. Kretzschmar, *Langmuir*, 2012, **28**, 1149–1156.
49 M. M. van Oene, L. E. Dickinson, F. Pedaci, M. Köber, D. Dulin, J. Lipfert and N. H. Dekker, *Phys. Rev. Lett.*, 2015, **114**, 218301.
50 C. A. Schneider, W. S. Rasband and K. W. Eliceiri, *Nat. Methods*, 2012, **9**, 671–675.
51 M. Mazars, *Phys. Rep.*, 2011, **500**, 43–116.
52 E. M. Furst and A. P. Gast, *Phys. Rev. E: Stat. Phys., Plasmas, Fluids, Relat. Interdiscip. Top.*, 2000, **62**, 6916–6925.
53 K. Butter, P. H. H. Bomans, P. M. Frederik, G. J. Vroege and A. P. Philipse, *Nat. Mater.*, 2003, **2**, 88–91.
54 M. Wang, L. He and Y. Yin, *Mater. Today*, 2013, **16**, 110–116.
55 F. Kogler, O. D. Velev, C. K. Hall and S. H. L. Klapp, *Soft Matter*, 2015, **11**, 7356–7366.
56 D. Morales, B. Bharti, M. D. Dickey and O. D. Velev, *Small*, 2016, **12**, 2283–2290.
57 S. R. Mishra, M. D. Dickey, O. D. Velev and J. B. Tracy, *Nanoscale*, 2016, **8**, 1309–1313.
58 A. Carlson, A. M. Bowen, Y. Huang, R. G. Nuzzo and J. A. Rogers, *Adv. Mater.*, 2012, **24**, 5284–5318.
59 R. M. Erb, J. S. Sander, R. Grisch and A. R. Studart, *Nat. Commun.*, 2013, **4**, 1712.

